Biochemical Journal (2020) **477** 2179–2192
https://doi.org/10.1042/BCJ20200238

PORTLAND PRESS

Research Article

Carrot 'antifreeze' protein has an irregular ice-binding site that confers weak freezing point depression but strong inhibition of ice recrystallization

Yannan Wang[1,*], Laurie A. Graham[2,*], Zhifu Han[3,*], Robert Eves[2], Audrey K. Gruneberg[2], Robert L. Campbell[2], Heqiao Zhang[1] and Peter L. Davies[2]

[1]Shanghai Institute for Advanced Immunochemical Studies (SIAIS), ShanghaiTech University, Shanghai 201210, China; [2]Department of Biomedical and Molecular Sciences, Queen's University, Kingston, ON, Canada K7L 3N6; [3]School of Life Sciences, Tsinghua University, Beijing 100084, China

Correspondence: Peter L. Davies (peter.davies@queensu.ca) and Heqiao Zhang (zhanghq@shanghaitech.edu.cn)

Ice-binding proteins (IBPs) are found in many biological kingdoms where they protect organisms from freezing damage as antifreeze agents or inhibitors of ice recrystallization. Here, the crystal structure of recombinant IBP from carrot (*Daucus carota*) has been solved to a resolution of 2.3 Å. As predicted, the protein is a structural homologue of a plant polygalacturonase-inhibiting protein forming a curved solenoid structure with a leucine-rich repeat motif. Unexpectedly, close examination of its surface did not reveal any large regions of flat, regularly spaced hydrophobic residues that characterize the ice-binding sites (IBSs) of potent antifreeze proteins from freeze-resistant fish and insects. An IBS was defined by site-directed mutagenesis of residues on the convex surface of the carrot solenoid. This imperfect site is reminiscent of the irregular IBS of grass 'antifreeze' protein. Like the grass protein, the carrot IBP has weak freezing point depression activity but is extremely active at nanomolar concentrations in inhibiting ice recrystallization. Ice crystals formed in the presence of both plant proteins grow slowly and evenly in all directions. We suggest that this slow, controlled ice growth is desirable for freeze tolerance. The fact that two plant IBPs have evolved very different protein structures to affect ice in a similar manner suggests this pattern of weak freezing point depression and strong ice recrystallization inhibition helps their host to tolerate freezing rather than to resist it.

Introduction

Antifreeze proteins (AFPs) were first discovered in Antarctic fishes in the late 1960s [1], and have since been found in many different biological kingdoms, including arthropods, plants, algae, fungi and eubacteria [2,3]. To date, about a dozen fundamentally different AFP structures have been solved, which itself implies their relatively recent evolution from different progenitor genes [4]. What is generally not known beyond the field is that these AFPs can serve different functions in different organisms. In fishes and insects, they protect the organism from freezing by binding to, and stopping further growth of internal seed ice crystals [5]. However, in plants that cannot resist freezing, AFPs appear to help the organism tolerate being frozen by preventing the recrystallization of ice [6]. In ice recrystallization, large ice crystals grow at the expense of small ones through the transfer of water across the ice grain boundaries [7]. This process can facilitate the dehydration of cells and cause structural damage to plant tissues [8,9]. Other AFP functions include the structuring of ice around microorganisms in sea ice to keep brine channels open [10]; and even the adhesion of bacteria to the ice to place them in a favourable environmental niche [11,12]. Because of this diversity in function, AFPs have

*Yannan Wang, Laurie A. Graham, Zhifu Han contributed equally to this work.

Received: 24 March 2020
Revised: 21 May 2020
Accepted: 27 May 2020

Accepted Manuscript online: 27 May 2020
Version of Record published: 22 June 2020

Biochemical Journal (2020) 477 2179–2192
https://doi.org/10.1042/BCJ20200238

recently been rebranded as ice-binding proteins (IBPs) [13]. Ice binding describes a more fundamental property of the protein that can encompass ice recrystallization inhibition (IRI) and ice adhesion in addition to antifreeze functions. Thus, all AFPs are IBPs, but only some IBPs, those that prevent their host organism from freezing, should be called AFPs. IBPs have highly diverse structures, but all have a surface that binds to ice.

The structural basis for why some IBPs are used to resist freezing (AFPs) and others to tolerate freezing remains unknown. Even single amino acid changes on the ice-binding site (IBS) of an IBP structure can have significant effects on antifreeze activity as measured by thermal hysteresis (TH) in a nanolitre osmometer [14]. TH is the temperature difference between the depressed freezing point and the slightly elevated melting point that results from the adsorption of IBPs to the ice crystal surface [15,16]. Fish AFPs typically have moderate TH activities of 1–1.5°C at low concentrations (millimolar) [17]. These TH levels, along with the colligative effects of blood solutes, are sufficient to depress the freezing point of fishes down to, and beyond, that of seawater at −1.9°C. However, terrestrial insects can face much lower winter temperatures, and have generally evolved more potent AFPs, which have been referred to as 'hyperactive' [18]. TH measurements *in vitro* for insect AFPs by freezing point osmometry can attain 6°C [19]. The key to hyperactivity appears to be the AFP's ability to bind to the basal plane of ice [20]. Moderately active fish AFPs bind only to the prism and/or pyramidal planes of ice to form hexapyramidal-shaped crystals.

Research into plant IBPs has lagged behind that in animals. We know that many higher plants have IBPs and that they exist as many different structural types [21,22]. However, only a few, such as those from bittersweet nightshade [23], carrot [6] and grass [24], have been purified and characterized; and of these the only available crystal structure is that of an IBP from perennial ryegrass, *Lolium perenne* [25]. In contrast with fish and insect AFPs, plant IBPs have maximal TH activities of only half a degree Celsius, and yet are highly active in IRI [24,26]. The molecular basis for this property (high IRI, but low TH) is difficult to deduce from one structure. *L. perenne* IBP (*Lp*IBP) folds as a single beta-solenoid, as do many of the insect and microorganism IBPs [4]. Its IBS on one face of the protein has been identified by site-directed mutagenesis [27]. In contrast with the insect AFPs like those from *Tenebrio molitor* (*Tm*AFP), spruce budworm (sbwAFP) and *Rhagium inquisitor* (*Ri*AFP) [28–30], which have two or more regular ranks of threonine residues that may organize ice-like waters on their IBSs, the equivalent IBS on *Lp*IBP is heavily substituted with Ser, Val, Ile, Asn and Ala residues [25]. These substitutions in other AFPs are known to reduce TH activity [31–33]. With just a single example on which to base explanations, we have pursued here the crystal structure of carrot (*D. carota*) IBP (*Dc*IBP) to see if a pattern emerges.

*Dc*IBP was first purified by conventional methods from cold-acclimated taproots [6,34] as a 36-kDa secreted glycoprotein. It was detected and purified based on its ice recrystallization activity. Removal of the small N-linked glycan chains did not negatively affect the IRI activity used to track the protein's purification [26]. Peptide sequences from the IBP were used to access DNA clones from which the full-length, 332-residue, preprotein sequence was derived. The first 26 residues serve as a signal sequence [6,34]. The mature protein is a homologue of plant polygalacturonase inhibitor proteins (PGIPs) which possesses leucine-rich repeat (LRR) motifs and is secreted into the apoplast to counteract degradative enzymes from plant pathogens [35,36]. The LRR beta-solenoid structure of PGIP2 from the green bean, *Phaseolus vulgaris*, which shares 42.7% identity with *Dc*IBP [37], was used to homology model the carrot protein [38].

Here, we report the X-ray crystal structure of *Dc*IBP produced by recombinant methods. Although this experimentally determined structure agrees well with a previous homology model [38], we have located the IBS on a completely different surface of the protein compared with the one predicted from the model. The IBS is small and irregular, which befits an IBP with weak TH activity. Our characterization of this IBP structure highlights a remarkable example of convergent evolution to a common function, where two different plants, grass and carrot, have used structurally unrelated proteins to develop imperfect IBSs that avoid super-cooling the plant, and yet still have high IRI activity to help their hosts tolerate freezing.

Materials and methods

Protein expression and purification

Full-length mature *Dc*IBP (306 residues without the signal sequence) was amplified from a carrot cDNA library and first cloned into pFastBac-1 vector with two alanines followed by a hexa-histidine tag at its C terminus to facilitate purification. The calculated mass of the His-tagged *Dc*IBP without glycosylation, with all cysteines disulfide-bonded, and with an N-terminal pyroglutamyl group was 34 932 Da. Subsequently, insertion of the

same construct into the Multi-Bac vector pKL improved the protein yield. The latter construct was confirmed by DNA sequencing and then transfected into DH10EMBacY competent cells. *Dc*IBP recombinant bacmids were extracted and transformed into sf9 insect cells using the standard Bac-to-Bac baculovirus expression system (Invitrogen). High Five cells (1 l of 2.0×10^6 cells ml^{-1}) were infected with a baculovirus inoculum (15 ml). After 72 h of infection, the medium containing the secreted *Dc*IBP was harvested and the His-tagged protein was recovered on Ni-NTA resin (GE Healthcare). The *Dc*IBP was further purified using size-exclusion chromatography (HiLoad 200, 16/600, GE Healthcare) in a buffer containing 20 mM Bis-Tris (pH 6.0) in 100 mM NaCl. Mutants were produced using the QuikChange Site-Directed Mutagenesis Kit (Stratagene) and confirmed by sequencing. The expression and purification procedures for all *Dc*IBP mutants were performed the same way as for the wild-type protein. For crystallization screening, the wild-type *Dc*IBP was concentrated to 10 mg/ml.

Crystallization, data collection, structure determination and refinement

Crystallization screening was performed at 18°C by the hanging-drop vapour-diffusion method. Diffraction quality crystals of *Dc*IBP were obtained by mixing 1 µl each of the protein and a reservoir solution containing 0.2 M sodium malonate (pH 4.0), and 20% w/v polyethylene glycol 3350. To lessen radiation damage from the X-ray beam, crystals were flash frozen using a reservoir buffer containing 12% glycerol as the cryoprotectant. Diffraction data sets were collected at the Shanghai Synchrotron Radiation Facility (SSRF) on beam line BL17U1. The data were processed using the HKL2000 software package [39]. The crystal structure of *Dc*IBP was determined by molecular replacement performed using PHASER [40] with the PGIP2 structure (PDB code: 1OGQ) serving as the initially search model. The initial model of *Dc*IBP obtained from molecular replacement was built with the program COOT [41,42] and then subjected to refinement by the program Phenix [43] and Refmac [44]. All structure figures shown in this manuscript were prepared using PyMOL (The PyMOL Molecular Graphics System, Version 2.0 Schrödinger, LLC).

Assays of TH, ice crystal shaping and IRI

TH of *Dc*IBP and its mutants were measured as previously described [45,46]. Briefly, protein samples, in 10 mM Bis-Tris (pH 6.0) and 100 mM NaCl, were suspended in Type B immersion oil as droplets and cooled on a Clifton nanoliter stage using a Newport model 3040 temperature controller. Upon obtaining a single ice crystal, the temperature was decreased below the melting point by 0.005°C every 4 s. Images and videos of ice crystal bursts and ice crystal shaping were captured using a Panasonic WV-BL200 digital camera. Videos were recorded at 30 frames/s. IRI assays were done by flash-freezing a series of 10-fold dilutions of IBP samples in thin wells within a super hydrophobic coating on sapphire slides, using the Tris-containing buffer, as described in [47]. The only differences were that the annealing temperature used was −6°C, rather than −5.3°C, and the sapphire slides were optically neutral (*c*-axis perpendicular to the plane of the slide) so they required no alignment prior to viewing through crossed polarizers. Samples were evaluated by noting the lowest concentration at which recrystallization did not occur.

Circular dichroism measurements

The wild-type and mutant T183Y *Dc*IBPs, at concentrations of 29 µM and 25 µM respectively, were dialyzed against 10 mM Tris–HCl (pH 8.0). Each sample was scanned seven times at 4°C with a Chirascan CD Spectrometer (Applied Photophysics, Leatherhead, Surrey, U.K.). The scans from each sample were averaged, the buffer signal was subtracted, and three-point smoothing was applied with Proviewer software. The deconvolution of the spectra was performed with OLIS SpectralWorks (On-Line Instruments, Bogart, GA, U.S.A.).

Results

DcIBP has weak TH activity

Recombinant *Dc*IBP was produced in the insect cell expression system and purified to homogeneity as described in Materials and methods. When tested at two concentrations, 12 µM (0.42 mg/ml) and 37 µM (1.26 mg/ml), wild-type *Dc*IBP had TH activities of 0.10°C and 0.15°C, respectively (Table 1). The trajectory of this TH activity as a function of protein concentration suggests that it will reach plateau activity values at or below 0.5°C. This is weak TH activity, on a par with that seen for grass IBP (*Lp*IBP) [27], and considerably less activity than that seen with the moderately active fish AFPs [17]. The other indication of weak activity is the

Biochemical Journal (2020) 477 2179–2192
https://doi.org/10.1042/BCJ20200238

Table 1. TH values of wild-type *Dc*IBP and mutants

Protein	TH at 12 μM (0.42 mg/ml)	TH at 37 μM (1.26 mg/ml)	TH at 66 μM (2.31 mg/ml)
WT	0.097 ± 0.008	0.15 ± 0.02	N/A
N299K	0.095 ± 0.005	0.157 ± 0.011	0.187 ± 0.011
A194Y	0.077 ± 0.006	N/A	N/A
Q165Y	0.073 ± 0.005	N/A	N/A
L140Y	0.067 ± 0.006	N/A	N/A
Q205A/T207A	0.055 ± 0.005	N/A	N/A
L159A/V161K	0 ± 0	N/A	N/A
T183Y	0 ± 0	N/A	N/A

Standard deviation was calculated from three readings.

nature of the ice crystal 'burst' once the depressed freezing point is exceeded. Ice crystals in the presence of *Dc*IBP grow steadily in all dimensions with evidence of faceting (Figure 1B). This same behaviour is also seen with *Lp*IBP [27], whereas ice crystals bound by moderately active fish AFPs grow rapidly out of their bipyramidal tips along the *c*-axis, and ice crystals limited by hyperactive IBPs 'burst' suddenly along their *a*-axis.

Despite its weak freezing point depression, DcIBP has strong IRI activity

The relationship between TH and IRI has not yet been deduced. Clearly, the ability to adsorb to the surface of ice is essential for both activities. However, it is not obvious that an IBP with high TH activity will have high IRI activity and vice versa. Indeed, the initial reports on the grass IBP, *Lp*IBP, suggested that this IBP had potent IRI activity but very weak TH [24]. Here, we have tested this relationship with *Dc*IBP. Although wild-type carrot IBP has feeble TH activity, multiple 10-fold dilutions of a stock solution indicates that it has exceptional IRI activity down to 37 nM (Figure 2). This is IRI activity of a similar order of magnitude to that observed with the bacterial IBP, *Sf*IBP, which is one of the most potent ice recrystallization inhibitors we have tested [48].

Carrot ice-binding protein (DcIBP)is a curved beta-solenoid

After X-ray diffraction data collection, the crystal structure at 2.3 Å resolution was determined by molecular replacement using the co-ordinates of PGIP2 (PDB code: 1OGQ) from *P. vulgaris*, as the search model (Table 2). A total of 304 out of the 306 residues within the mature *Dc*IBP were successfully assigned (Figure 3). The density corresponding to the first two residues would not permit an unambiguous assignment. Like its homologues in the plant leucine-rich region (LRR) receptor-like kinase family, *Dc*IBP adopts a right-handed super-helical solenoid structure containing 10 LRRs. The central repetitive section is flanked by two capping regions, both of which have two pairs of disulfide-bonded cysteines. The N-terminal cap of ∼50 residues is more extensive than the C-terminal cap. The solenoid has a pronounced curvature, with the concave surface occupied by an extensive beta-sheet (Figure 3B). Almost directly opposite on the convex surface are nine 3_{10}--helices. We also observed that *Dc*IBP was N-glycosylated at N294 (asparagine 294).

The LRRs of *Dc*IBP contain conserved residues (Figure 4A), most of which are hydrophobic and form the core of the solenoid (Figure 4B). The aliphatic and aromatic residues (green or blue) frequently stack with their counterparts on neighbouring LRRs. In addition, there are conserved internal asparagines at eight positions (purple, Figure 4A), which form a ladder where both the oxygen and nitrogen of the carboxamide group make hydrogen bonding interactions with the peptide backbone (Figure 4C). These bonds occur both within the loop containing the asparagine and to the previous loop. The conserved glycine (orange) forms a turn and the conserved proline (red) affects the pitch of the 3_{10} helix so that the 3rd and 6th residue following face inward (Figure 4A, LRR1-6).

As would be expected from the success of molecular replacement, the crystal structure of *Dc*IBP is a close match to that of PGIP2 (Figure 5A). The two mature sequences share 42.7% identity, with 100% conservation of the eight cysteines involved in disulfide bonds, high conservation of the asparagine ladder and good

Biochemical Journal (2020) **477** 2179–2192
https://doi.org/10.1042/BCJ20200238

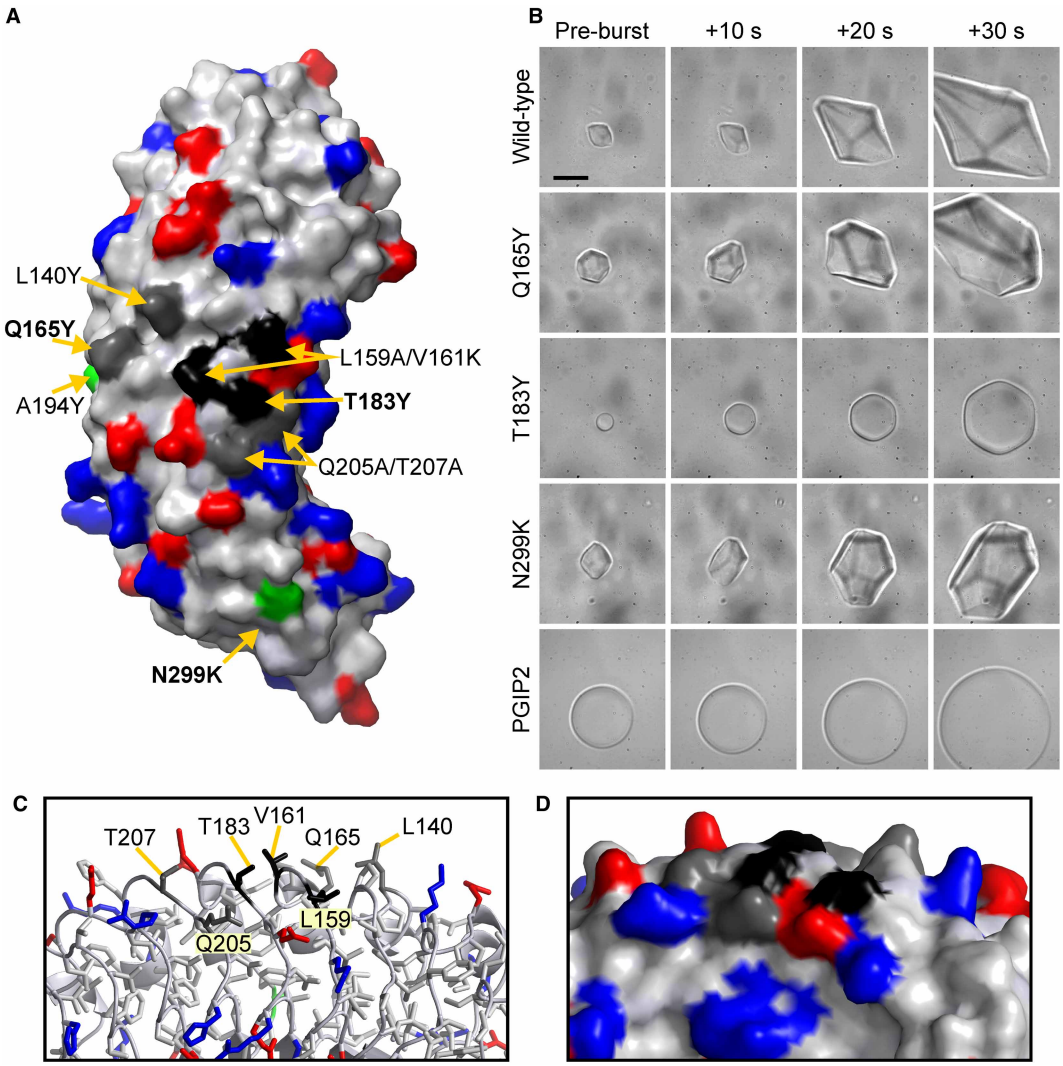

Figure 1. Mutagenesis to determine the ice-binding site of carrot IBP.

(**A**) Space-filling representation of the carrot IBP. Negatively charged residues are shown in red and positively charged residues are coloured blue. Mutated residues are denoted by their one-letter code and number followed by the code of the residue to which it was changed. Colour for these residues is used to indicate whether the mutation(s) had a severe (black), moderate (grey) or minor (green) effect on activity. (**B**) Images of single crystals generated in the presence of wild-type *Dc*IBP, three mutations indicated in bold in (**A**), and recombinant PGIP2 at 18 mg/ml. The pre-burst image is taken just before the non-equilibrium freezing point is reached and the subsequent images at 10 s intervals thereafter while cooling at a rate of 0.075°C/min. Note that T183Y and PGIP2 had no detectable TH so ice crystals in their presence grew uniformly without a burst point. The black scale bar on the top left image is 20 μm long and the scale is the same for all images. (**C**) Close-up of the ice-binding site showing its residues in ribbon and stick presentation. (**D**) The same view as in (**C**) but in space-filling mode to illustrate its flatness.

conservation of the hydrophobic core residues (Supplementary Figure S1). These two structures were well superposed with a root mean square deviation of 0.874 Å over 297 Cα atoms. Both proteins have the parallel beta-sheet that lies on the concave site of the solenoid. The two capping structures, including the four disulfide bonds, also overlapped well.

DcIBP has an IBS centred on T183

Given that *Dc*IBP is a curved solenoid (Figure 3), there are few obviously flat surfaces that could serve as an IBS. Visual inspection of the protein suggested there were three small regions that were somewhat flat and less

Biochemical Journal (2020) 477 2179–2192
https://doi.org/10.1042/BCJ20200238

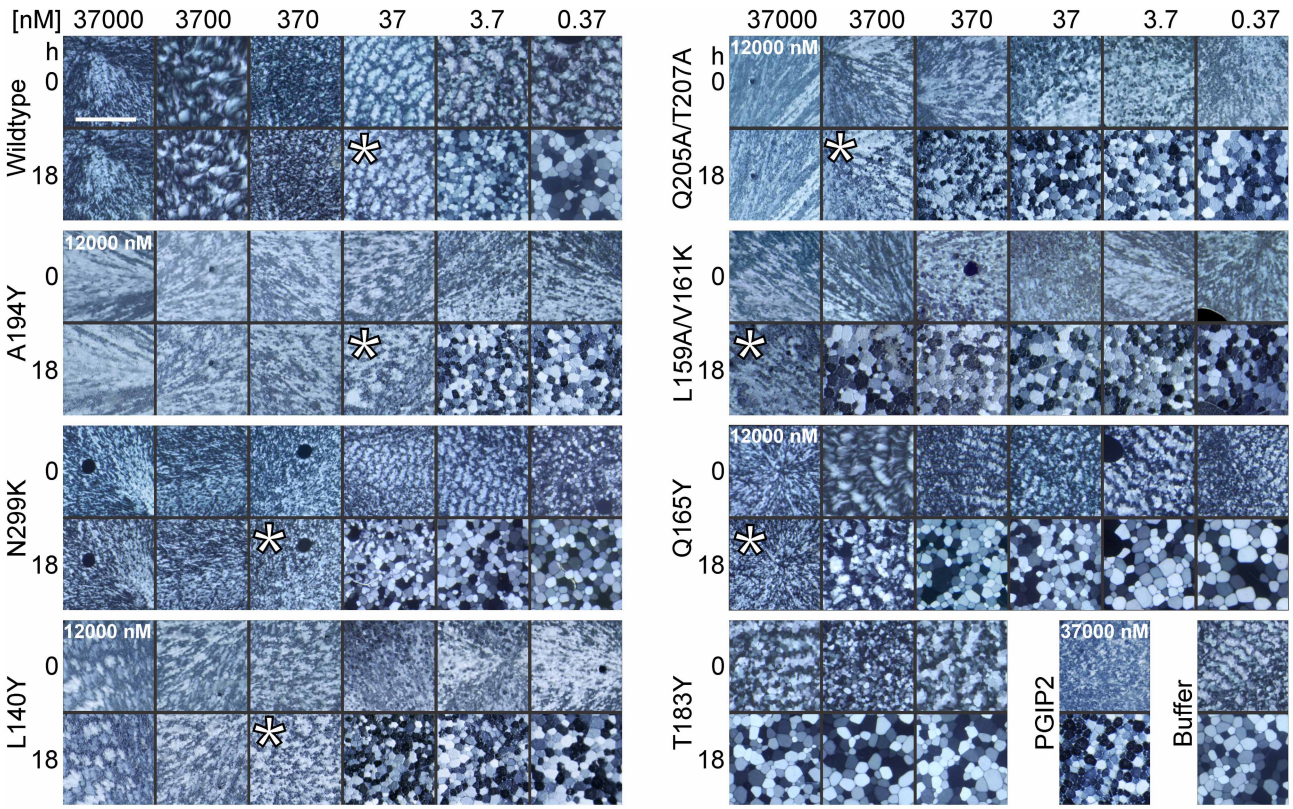

Figure 2. IRI activity of carrot IBPs and controls.

The wild-type or mutant protein being assayed in each horizontal set of images is identified on the left side of the panel. The protein concentrations tested (nM) in a 10-fold dilution series from left to right are listed along the top of the figure. Exceptions from these dilutions are identified by IBP concentration within a specific image. The top panel of six images in each dilution series shows the ice pattern shortly after the sample was flash frozen, whereas the bottom set shows it after 18 h of incubation at −6°C. The white asterisk marks the IRI endpoint (the last dilution at which complete IRI is observed). The two lowest dilutions of mutant T183Y have been omitted to make room for the PGIP2 sample and the buffer control. The 1 mm size marker is shown in the top left panel.

charged than the rest of the protein (Supplementary Movie). To probe these regions for their ice-binding capability, mutations were made to introduce a bulkier outfacing side chain at the centre of each site, specifically Q165Y, T183Y and N299K (Figure 1A). We then compared the TH activity of these mutants to that of the wild type at the same protein concentration. At 12 μM, the wild-type and N299K had similar TH activities of 0.097 ± 0.008°C and 0.095 ± 0.005°C, respectively. Mutant N299K also showed similar activity to wild-type *Dc*IBP when tested at 37 μM, with TH values of 0.16°C and 0.15°C, respectively (Table 1).

The activity of Q165Y was ∼25% reduced to 0.073 ± 0.005°C, whereas T183Y was completely inactive (Table 1). Consistent with these TH activity differences, the ice crystals formed in the presence of wild-type *Dc*IBP and active mutants Q165Y and N299K were heavily faceted and resembled incompletely extended hexagonal bipyramids (Figure 1B). In contrast, the ice crystals formed in the presence of the T183Y mutant were circular discs like those formed in the absence of IBPs [17], but with a slight amount of hexagonal shaping.

These mutants were also evaluated for IRI activity in which a series of 10-fold dilutions were tested in the modified splat assay (Figure 2). In the dilution series of the wild type shown in the top, left-hand panels there was no difference in the ice crystal patterns of each dilution over 18 h down to 37 nM. With a further 10-fold dilution to 3.7 nM, the ice crystals grew slightly, indicating that while recrystallization was not prevented, it was slowed down. Upon a further 10-fold dilution to 0.37 nM, there was a pronounced increase in ice crystal size over 18 h, as there was in the buffer control. The N299K mutation showed a slight activity loss relative to *Dc*IBP as it was only effective down to 370 nM rather than 37 nM. Concordant with their TH activity differences, the Q165Y mutant was significantly less active again as its endpoint was 12 000 nM. In contrast, the

Biochemical Journal (2020) **477** 2179–2192
https://doi.org/10.1042/BCJ20200238

Table 2. Data collection and refinement statistics

	***Dc*IBP**
Data collection	
Space group	P $2_12_12_1$
Cell dimensions *a*, *b*, *c* (Å)	38.89, 57.45, 135.54
Resolution (Å)	50–2.30 (2.34–2.30)
R_{meas}	12.7 (49.1)
I/σ (I)	16.77 (8.51)
Completeness (%)	100.0 (99.8)
Redundancy	8.8 (9.0)
Refinement	
Resolution (Å)	37.41–2.31 (2.37–2.31)
No. reflections	13 160
R_{work} (%)	16.5 (17.0)
R_{free} (%)	22.3 (26.8)
No. atoms	
Protein	2425
Water	115
r.m.s. deviations (bonds)	0.0161
r.m.s. deviations (angles)	2.117
Average B-factor	39.7
Ramachandran favoured	91.9%
Ramachandran outliers	0.3%

T183Y mutant showed no IRI activity whatsoever. Even at 37 000 nM, the highest concentration tested, this mutant failed to prevent or even slow the growth of ice crystals (Figure 2, lower right-hand panels). It was equivalent in this respect to the buffer control.

One of the key checks to make when evaluating the loss of activity of a protein as a result of mutagenesis is to ensure that the protein is properly folded. All the mutated *Dc*IBP residues have side chains that project outward to the solvent and should not interfere with the protein fold. Nevertheless, to ascertain this for T183Y, the most severe mutant lacking both TH and IRI activity, we performed circular dichroism (CD) analysis. The CD spectrum of T183Y perfectly overlapped with that of the wild-type *Dc*IBP having a molar ellipticity maximum at 198 nm and a minimum at 218 nm (Supplementary Figure S2A) indicating that their folds were the same.

The DcIBP IBS occupies a small area of the protein

To determine the extent of the IBS, additional mutations were introduced in the vicinity of T183 (Figure 1A) and their TH activity (Table 1) and IRI activity (Figure 2) were measured. The mutation A194Y, which is the farthest away from T183 in this series, had only a minor effect on TH activity (20% loss), but the IRI endpoint remained at 37 nM. The L140Y mutation, which is slightly closer to T183, showed a 30% loss in TH relative to A194Y (0.067 vs 0.077°C), and small loss of IRI activity as the endpoint shifted to 370 nM. When the two surface residues immediately flanking T183 in the direction of L140 and A194 were mutated (L159A/V161K), TH was zero, but some IRI activity remained as it was effective at the highest concentration tested (37 000 nM). Removal of the two polar side chains on the opposite side of T183 (Q205A/T207A) also had a moderate effect with TH activity reduced to 0.055°C (40% loss) and the IRI endpoint of 3700 nM was intermediate between that of the double mutant L159A/V161K and the single mutant L140Y. In summary, the rank order of TH activity was wild type, N299K, A194Y, Q165Y, L140Y, Q205A/T207A, L159A/V161K and T183Y. The latter two mutants had no perceptible TH activity, and Q205A/T207A had about half the TH activity of the wild-type

Biochemical Journal (2020) **477** 2179–2192
https://doi.org/10.1042/BCJ20200238

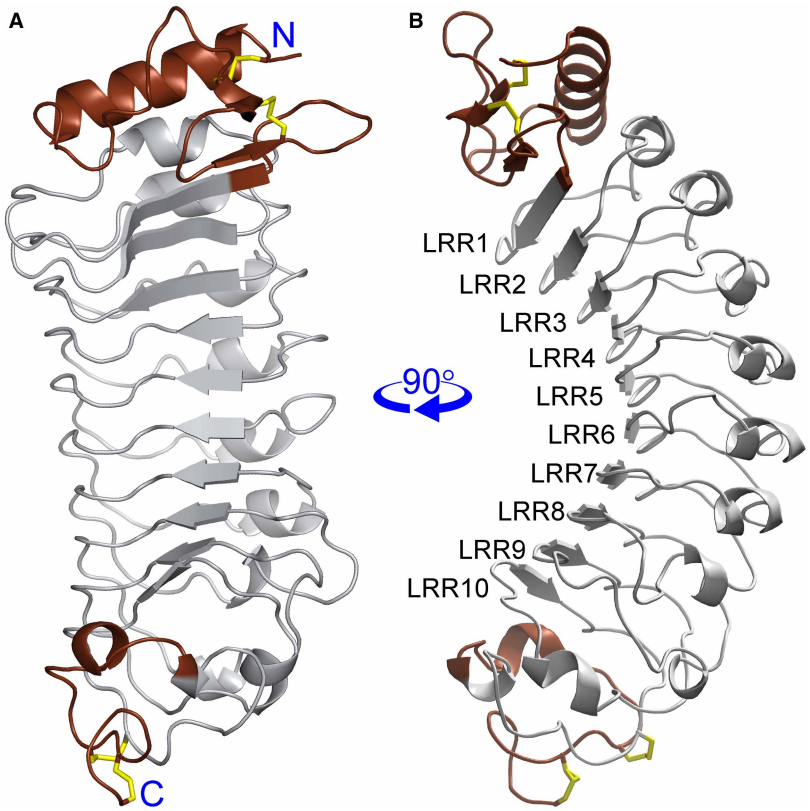

Figure 3. Cartoon representation of the crystal structure of carrot IBP (*Dc*IBP).

The N- and C-terminal capping structures are in brown and the ten leucine-rich repeats (LRRs) numbered on the right are in grey. Disulfide bonds (four total) are shown in yellow, two in each capping structure. (**A**) The concave beta-stranded surface of the solenoid is shown facing the viewer. (**B**) A 90° rotation of the left-hand image about the vertical axis with the beta-strands on the left and the 3_{10} helices on the right.

*Dc*IBP. N299K had the same TH activity as the wild-type *Dc*IBP (Table 1). Taken together, these results indicate that the IBS occupies a relatively small region of the surface of the protein, in the vicinity of T183.

We also compared the IRI activity of the *Dc*IBP mutants to see if they lost IRI activity in rank order relative to the loss of TH activity. The rank order of IRI activity was wild type ≈ A194Y, N299K ≈ L140Y, Q205A/T207A, Q165Y ≈ L159A/V161K and T183Y, which spanned a concentration range of at least three orders of magnitude from 37 nM to over 37 000 nM. In comparison, the rank order of TH activity was wild type ≈ N299K, A194Y, Q165Y, L140Y, Q205A/T207A and L159A/V161K ≈ T183Y. This is a similar order but for the reversal of A194Y and N299K, and the higher ranking of Q165Y, in the TH series, indicating that there is a general positive correlation between TH and IRI activity for *Dc*IBP.

Functional differences between PGIP2 and DcIBP lie in their surface residues

The main difference between *Dc*IBP and its polygalacturonase inhibitor protein (PGIP2) homologue lies in the surface residues, which is consistent with the fact that they have different functions. *Dc*IBP has a neutral patch on the edge of the top surface which we have identified here as ice binding, whereas the same region in PGIP2 is more charged (Figure 5B,C) with an aspartic acid at position 148 (Supplementary Figure S1). Conversely, PGIP2 possesses a pronounced negatively charged pocket on the concave solenoid surface, which is involved in the recognition and binding of polygalacturonases (Figure 5C) [49]. In *Dc*IBP a cluster of basic amino acids, R105, K106 and R128, completely reverses the charge within the middle of this pocket. This helps explain why *Dc*IBP and PGIP2 have totally different functions as previously reported [6,34,37]. When recombinant PGIP2 at 18 mg/ml (515 μM) was tested for TH activity in this study it was completely devoid of antifreeze activity (Figure 1) and was unable to even shape ice crystals.

Biochemical Journal (2020) **477** 2179–2192
https://doi.org/10.1042/BCJ20200238

A

```
mniessfcpilcicmiflclpnlsas  26 signal peptide
QRCNNNDKQALLQIKTALKNPTITD   51
SWVSDDDCCGWDLVECDETSNRII    75 N-terminal cap

#      Concave Side    Convex      Side
LRR1   SLIIQD  DEALT   GQIPPQVGDL  PYLQ   100 (25)
LRR2   ALWFRK  LPNLF   GKIPEEISAL  KDLK   125 (25)
LRR3   SLRLSS  TS-LS   GPVPLFFPQL  TKLT   149 (24)
LRR4   CLDLSF  NK-LL   GVIPPQLSTL  PNLK   173 (24)
LRR5   ALHLER  NE-LT   GEIPDIFGNF  AGSP   197 (24)
LRR6   DIYLSH  NQ-LT   GFVPKTFARA  -DPI   220 (23)
LRR7   RLDFSG  NR-LE   GDISFLFGPK  KRLE   244 (24)
LRR8   MLDFSG  NV-LS   FNFSRVQEFP  PSLT   268 (24)
LRR9   YLDLNH  NQ-IS   GSLSSELAKL  -DLQ   291 (23)
LRR10  TFNVSD  NN-LC   GKIPTG----  GNLQ   311 (20)
       RFDYLH  NSCLC   GAPLPEC             332 (21)
         ^
       RTA     C-terminal cap
```

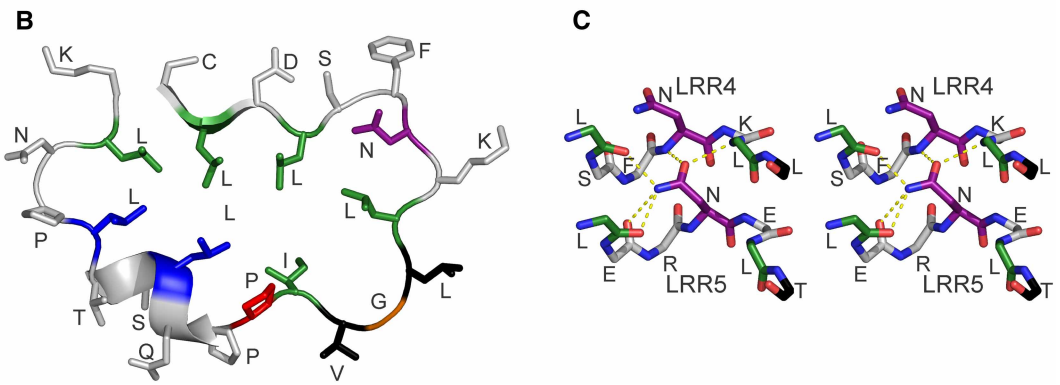

Figure 4. LRRs of carrot IBP.

(**A**) Sequence of the carrot IBP precursor with LRRs 1 to 10 aligned. Residues with outward projecting side chains are in light grey. Inward projecting residues at positions within the repeats are coloured as follows; high Asn content (purple), Leu/Ile content greater than 50% (green) and less than 50% (blue). Conserved Gly (plus one Phe) are orange and conserved Pro are red. Cys involved in disulfide bonds are highlighted yellow, the signal peptide is in lower-case font and the capping residues are coloured brown. Residues that were mutated to map the ice-binding site are underlined, and those with a severe effect are coloured black with double underlining. Mutations with a moderate effect are coloured dark grey and those shown in light grey were mild or had no effect. (**B**) Cartoon representation in stick format of LRR4 with all side chains shown and coloured as in (**A**). (**C**) Stereo stick diagram of the hydrogen bonding network between Asn180 in LRR5 with neighbouring residues in LRR4 (top) and LRR5 (bottom), with carbon atoms coloured as in (**A**) but with oxygen in red and nitrogen in blue. The side chains of non-Asn residues are omitted for clarity.

DcIBP differs in several ways from other beta-solenoid IBPs

*Dc*IBP is similar to at least six other IBPs in that it is a repetitive beta-solenoid [4]. The CD spectrum of this protein resembles quite closely those of three other repetitive beta-solenoid IBPs taken from the literature

Biochemical Journal (2020) **477** 2179–2192
https://doi.org/10.1042/BCJ20200238

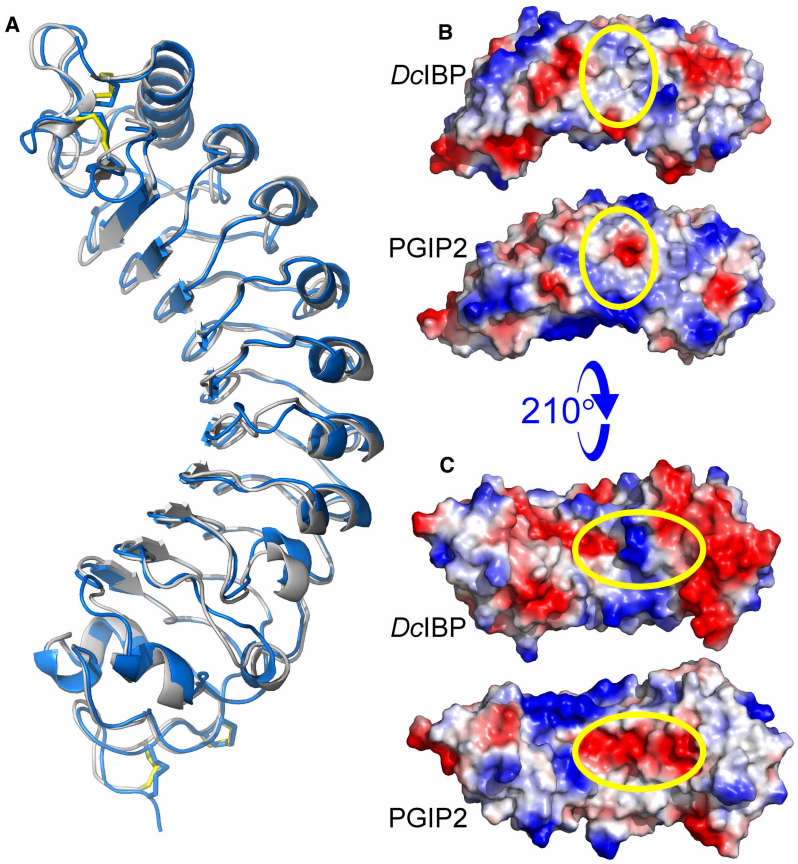

Figure 5. Comparison of carrot IBP with bean PGIP2.

(**A**) Superimposition of the cartoon representations of the IBP (grey) on PGIP2 (blue). The disulfide bonds of the IBP and PGIP2 are in yellow and blue, respectively. (**B**) The two proteins, *Dc*IBP (top) and PGIP2 (bottom), are displayed in space-filling mode with the average negative charge over a small region coloured red and average positive charge over a small region coloured blue. The ice-binding region of the IBP and the corresponding region of PGIP2 are encompassed by the yellow ellipses. (**C**) A 210° rotation of the renderings in (**B**) about the horizontal axis with the polygalacturonase binding pocket of PGIP2 and its equivalent area in *Dc*IBP indicated in the same manner.

(Supplementary Figure S2B), with maxima at ∼195 nm and troughs at ∼220 nm. However, *Dc*IBP differs from these other IBPs in one important way. The LRRs contain a thinner strand that lies on one side of the protein and a wider 3_{10} helix that lies on the other side (Figure 3). This arrangement introduces far more curvature than that found in other repetitive IBPs. Consequently, *Dc*IBP cannot accommodate a large, flat IBS, unlike the other solenoidal IBPs, such as those from bacteria, grass and several insects (Figure 6).

Discussion

Here, we have solved the crystal structure of a second plant IBP and located its IBS centred on surface residue T183 and the adjacent outward-pointing L159 and V161, and encompassing nearby residues L140, Q165, Q205 and T207. Residues A194 and N299 are far enough removed from the IBS to have little to no effect on the TH and IRI activity. One other supporting piece of information about the IBS is that glycosylation at the principal N-linked site N294 [34] does not affect the protein's ice-binding ability. N294 is far removed from the IBS and this effectively serves as having a mutation in another location.

A previous study accurately formed a homology model for the carrot IBP based on PGIP2 [38]. The IBS of *Dc*IBP in this report was centred on a conserved row of asparagines across eight neighbouring solenoid coils. We were sceptical of this claim because the identified Asn residues point inwards to form an asparagine ladder that is an integral part of the protein core and the protein fold. Also, the neighbouring residues that point

Biochemical Journal (2020) **477** 2179–2192
https://doi.org/10.1042/BCJ20200238

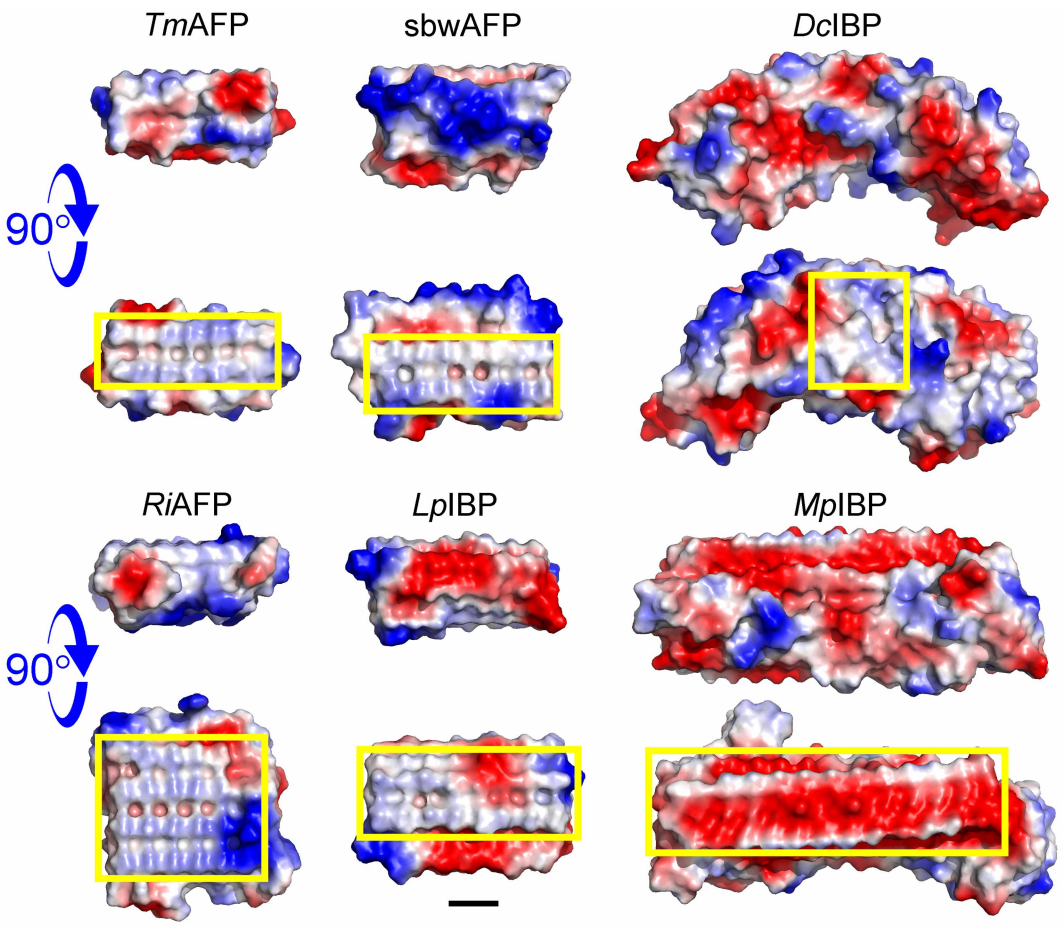

Figure 6. Comparison of the relative sizes of IBPs and their IBSs.

Six IBPs identified by their PDB codes (*Tm*AFP 1EZG; sbwAFP 1M8N; *Dc*IBP 6W78; *Ri*AFP 4DT5; *Lp*IBP 3ULT; and *Mp*IBP 3P4G) are shown in electrostatic surface representation with electrostatic potential coloured from red (most negative) through white (neutral) to blue (most positive). The upper figures are side-on views, and the lower image of the pair has been rotated through 90° to show the IBS bounded by a yellow rectangle. The scale bar at the bottom represents 10 Å.

outward are not in any way conserved between the LRRs. Furthermore, several flanking residues are charged, and charged residues are typically not found on an IBS [4]. The fact that mutation of these internal Asn residues to Val or Gln decreased TH activity of *Dc*IBP could reflect some disruption of the protein fold that would not necessarily be picked up by simple fluorescence spectroscopy.

Indeed, the possibility of finding extensive parallel arrays of ice-binding residues akin to the Thr-X-Thr seen in the insect AFPs like *T. molitor* (PDB entry: 1EZG) [28], *Choristoneura fumiferana* (PDB entry: 1M8N) [29] and *R. inquisitor* (PDB entry: 4DT5) [30], or the Thr-X-Asn in *Mp*AFP [50] and even the other plant IBP structure [25] is made unlikely by the pronounced curvature of the *Dc*IBP solenoid structure. The concave surface of *Dc*IBP would be the most difficult to fit to ice. The flanks of the solenoid fold are flatter, but form arcs that prevent the formation of parallel arrays of residues. The convex surface is fully accessible to ice but, because of its curvature, can only have a limited flat surface area. Instead, the IBS is an irregular patch of residues more like those on the globular type II and type III AFPs from fish [51,52]. Indeed, the central T183 residue on the *DcIBP* IBS is similar in importance to T18 on type III AFP, where replacement with Tyr eliminates TH activity [14].

Why does *Dc*IBP have such a small, imperfect IBS? This might reflect selection for an IBP with low TH activity. The idea here would be for plants to freeze in a slow, controlled way, rather than after a considerable depression of the freezing point that would lead to explosive ice growth in many directions, with rapid volume

Biochemical Journal (2020) **477** 2179–2192
https://doi.org/10.1042/BCJ20200238

expansion and shearing from ice shards causing structural damage to the plant. This is the opposite strategy adopted by fish and insect AFPs, where all the emphasis is on attaining adequate freezing point depression. If this value is insufficient to prevent freezing, the organism will die.

The first plant IBP to have its structure solved was that from the grass, *L. perenne* [25]. *Lp*IBP is a flat beta-solenoid of 14- or 15-residue coils with no obvious progenitor. It is remarkable that these two different proteins have the same properties of weak TH and strong IRI activity. Being a flat beta-solenoid, *Lp*IBP has the potential to host a regular array of parallel Thr-X-Thr motifs as seen in some hyperactive AFPs [28,29]. Instead, only 5 of 16 of the residues on the IBS are Thr. The others are uncharged residues (Ser, Val, Ile, Asn and Ala) which generate a more irregular surface than would a Thr array, and presumably attenuate the TH activity. Thus, these two plant IBPs have functionally converged to have low TH but high IRI activity.

There are likely to be more examples in the plant kingdom of IBPs that have evolved in this way, which need more detailed structural and bioinformatic analyses in the future. Of great interest in mechanistic terms is how these plant IBPs can have low TH activity and yet be very effective at IRI.

Database deposition

The atomic co-ordinates for the *Dc*IBP structure have been deposited in the PDB with accession number 6W78. The co-ordinates will be released on publication of this manuscript.

Competing Interests

The authors declare that there are no competing interests associated with the manuscript.

Funding

This work was supported by grants from the Natural Science Foundation of China [31700665] to H.Z. and [31971119] to Z.H., and by a CIHR Foundation award [FRN 148422] to P.L.D. P.L.D. holds the Canada Research Chair in Protein Engineering.

Author Contributions

H.Z., Z.H., L.A.G. and P.L.D. and designed the research. Y.W., H.Z., A.K.G. and R.E. performed experiments. Y. W., H.Z., R.L.C., L.A.G. and P.L.D. analyzed the data. Y.W., L.A.G. and P.L.D. wrote the manuscript. All authors reviewed and proof-read the manuscript.

Acknowledgements

We thank Prof. Jijie Chai for his great support at the early stage of this project. We also thank the staff of the BL17U1 (Wang et al., Nuclear Science and Techniques, 2018, 29(5):68) and BL19U1 beamlines at the National Center for Protein Sciences Shanghai (NCPSS) at SSRF. We are grateful to Kim Munro of the Protein Function Discovery Facility at Queen's University for assistance with CD measurements.

Abbreviations

AFP, antifreeze protein; CD, circular dichroism; IBP, ice-binding protein; IBS, ice-binding site; IRI, ice recrystallization inhibition; LRR, leucine-rich repeat; PGIP, polygalacturonase inhibitor protein; TH, thermal hysteresis.

References

1 DeVries, A.L. and Wohlschlag, D.E. (1969) Freezing resistance in some antarctic fishes. *Science* **163**, 1073–1075 https://doi.org/10.1126/science.163.3871.1073

2 Duman, J.G. (2015) Animal ice-binding (antifreeze) proteins and glycolipids: an overview with emphasis on physiological function. *J. Exp. Biol.* **218**, 1846–1855 https://doi.org/10.1242/jeb.116905

3 Bar Dolev, M., Braslavsky, I. and and Davies, P.L. (2016) Ice-binding proteins and their function. *Ann. Rev. Biochem.* **85**, 515–542 https://doi.org/10.1146/annurev-biochem-060815-014546

4 Davies, P.L. (2014) Ice-binding proteins: a remarkable diversity of structures for stopping and starting ice growth. *Trends Biochem. Sci.* **39**, 548–555 https://doi.org/10.1016/j.tibs.2014.09.005

5 DeVries, A.L. (1983) Antifreeze peptides and glycopeptides in cold-water fishes. *Annu. Rev. Physiol.* **45**, 245–260 https://doi.org/10.1146/annurev.ph.45.030183.001333

6 Worrall, D., Elias, L., Ashford, D., Smallwood, M., Sidebottom, C., Lillford, P., et al. (1998) A carrot leucine-rich-repeat protein that inhibits ice recrystallization. *Science* **282**, 115–117 https://doi.org/10.1126/science.282.5386.115

7 Knight, C.A., DeVries, A.L. and Oolman, L.D. (1984) Fish antifreeze protein and the freezing and recrystallization of ice. *Nature* **308**, 295–296 https://doi.org/10.1038/308295a0
8 Mazur, P. (1984) Freezing of living cells: mechanisms and implications. *Am. J. Physiol.* **247**, C125–C142 https://doi.org/10.1152/ajpcell.1984.247.3.C125
9 Thomashow, M.F. (1998) Role of cold-responsive genes in plant freezing tolerance. *Plant Physiol.* **118**, 1–8 https://doi.org/10.1104/pp.118.1.1
10 Raymond, J.A., Janech, M.G. and Fritsen, C.H. (2009) Novel ice-binding proteins from a psychrophilic antarctic alga (*Chlamydomonadaceae chlorophyceae*). *J. Phycol.* **45**, 130–136 https://doi.org/10.1111/j.1529-8817.2008.00623.x
11 Guo, S., Garnham, C.P., Whitney, J.C., Graham, L.A. and Davies, P.L. (2012) Re-evaluation of a bacterial antifreeze protein as an adhesin with ice-binding activity. *PloS One* **7**, e48805 https://doi.org/10.1371/journal.pone.0048805
12 Guo, S., Stevens, C.A., Vance, T.D.R., Olijve, L.L.C., Graham, L.A., Campbell, R.L., et al. (2017) Structure of a 1.5-MDa adhesin that binds its antarctic bacterium to diatoms and ice. *Sci. Adv.* **3**, e1701440 https://doi.org/10.1126/sciadv.1701440
13 Kang, J.S. and Raymond, J.A. (2004) Reduction of freeze-thaw-induced hemolysis of red blood cells by an algal ice-binding protein. *Cryo Lett.* **25**, 307–310 PMID: 15618982
14 DeLuca, C.I., Davies, P.L., Ye, Q. and Jia, Z. (1998) The effects of steric mutations on the structure of type III antifreeze protein and its interaction with ice. *J. Mol. Biol.* **275**, 515–525 https://doi.org/10.1006/jmbi.1997.1482
15 Duman, J.G. and DeVries, A.L. (1974) Freezing resistance in winter flounder. *Nature* **274**, 237–238 https://doi.org/10.1038/247237a0
16 Raymond, J.A. and DeVries, A.L. (1977) Adsorption inhibition as a mechanism of freezing resistance in polar fishes. *Proc. Natl. Acad. Sci. U.S.A.* **74**, 2589–2593 https://doi.org/10.1073/pnas.74.6.2589
17 Scotter, A.J., Marshall, C.B., Graham, L.A., Gilbert, J.A., Garnham, C.P. and Davies, P.L. (2006) The basis for hyperactivity of antifreeze proteins. *Cryobiology* **53**, 229–239 https://doi.org/10.1016/j.cryobiol.2006.06.006
18 Graham, L.A., Liou, Y.C., Walker, V.K. and Davies, P.L. (1997) Hyperactive antifreeze protein from beetles. *Nature* **388**, 727–728 https://doi.org/10.1038/41908
19 Duman, J.G. (2001) Antifreeze and ice nucleator proteins in terrestrial arthropods. *Annu. Rev. Physiol.* **63**, 327–357 https://doi.org/10.1146/annurev.physiol.63.1.327
20 Bar-Dolev, M., Celik, Y., Wettlaufer, J.S., Davies, P.L. and Braslavsky, I. (2012) New insights into ice growth and melting modifications by antifreeze proteins. *J. R. Soc. Interface* **9**, 3249–3259 https://doi.org/10.1098/rsif.2012.0388
21 Urrutia, M.E., Duman, J.G. and Knight, C.A. (1992) Plant thermal hysteresis proteins. *Biochim. Biophys. Acta* **1121**, 199–206 https://doi.org/10.1016/0167-4838(92)90355-H
22 Hon, W.C., Griffith, M., Chong, P. and Yang, D. (1994) Extraction and isolation of antifreeze proteins from winter rye (*Secale cereale* L.) leaves. *Plant Physiol.* **104**, 971–980 https://doi.org/10.1104/pp.104.3.971
23 Duman, J.G. (1994) Purification and characterization of a thermal hysteresis protein from a plant, the bittersweet nightshade *Solanum dulcamara*. *Biochim. Biophys. Acta* **1206**, 129–135 https://doi.org/10.1016/0167-4838(94)90081-7
24 Sidebottom, C., Buckley, S., Pudney, P., Twigg, S., Jarman, C., Holt, C., et al. (2000) Heat-stable antifreeze protein from grass. *Nature* **406**, 256 https://doi.org/10.1038/35018639
25 Middleton, A.J., Marshall, C.B., Faucher, F., Bar-Dolev, M., Braslavsky, I., Campbell, R.L., et al. (2012) Antifreeze protein from freeze-tolerant grass has a beta-roll fold with an irregularly structured ice-binding site. *J. Mol. Biol.* **416**, 713–724 https://doi.org/10.1016/j.jmb.2012.01.032
26 Smallwood, M., Worrall, D., Byass, L., Elias, L., Ashford, D., Doucet, C.J., et al. (1999) Isolation and characterization of a novel antifreeze protein from carrot (*Daucus carota*). *Biochem. J.* **340**, 385–391 https://doi.org/10.1042/bj3400385
27 Middleton, A.J., Brown, A.M., Davies, P.L. and Walker, V.K. (2009) Identification of the ice-binding face of a plant antifreeze protein. *FEBS Lett.* **583**, 815–819 https://doi.org/10.1016/j.febslet.2009.01.035
28 Liou, Y.C., Tocilj, A., Davies, P.L. and Jia, Z. (2000) Mimicry of ice structure by surface hydroxyls and water of a beta-helix antifreeze protein. *Nature* **406**, 322–324 https://doi.org/10.1038/35018604
29 Graether, S.P., Kuiper, M.J., Gagne, S.M., Walker, V.K., Jia, Z., Sykes, B.D., et al. (2000) Beta-helix structure and ice-binding properties of a hyperactive antifreeze protein from an insect. *Nature* **406**, 325–328 https://doi.org/10.1038/35018610
30 Hakim, A., Nguyen, J.B., Basu, K., Zhu, D.F., Thakral, D., Davies, P.L., et al. (2013) Crystal structure of an insect antifreeze protein and its implications for ice binding. *J. Biol. Chem.* **288**, 12295–12304 https://doi.org/10.1074/jbc.M113.450973
31 Chao, H., Houston, Jr, M.E., Hodges, R.S., Kay, C.M., Sykes, B.D., Loewen, M.C., et al. (1997) A diminished role for hydrogen bonds in antifreeze protein binding to ice. *Biochemistry* **36**, 14652–14660 https://doi.org/10.1021/bi970817d
32 Zhang, W. and Laursen, R.A. (1998) Structure-function relationships in a type I antifreeze polypeptide. The role of threonine methyl and hydroxyl groups in antifreeze activity. *J. Biol. Chem.* **273**, 34806–34812 https://doi.org/10.1074/jbc.273.52.34806
33 Haymet, A.D., Ward, L.G., Harding, M.M. and Knight, C.A. (1998) Valine substituted winter flounder 'antifreeze': preservation of ice growth hysteresis. *FEBS Lett.* **430**, 301–306 https://doi.org/10.1016/S0014-5793(98)00652-8
34 Meyer, K., Keil, M. and Naldrett, M.J. (1999) A leucine-rich repeat protein of carrot that exhibits antifreeze activity. *FEBS Lett.* **447**, 171–178 https://doi.org/10.1016/S0014-5793(99)00280-X
35 Cervone, F., De Lorenzo, G., Degra, L., Salvi, G. and Bergami, M. (1987) Purification and characterization of a polygalacturonase-inhibiting protein from *Phaseolus vulgaris* L. *Plant Physiol.* **85**, 631–637 https://doi.org/10.1104/pp.85.3.631
36 De Lorenzo, G. and Ferrari, S. (2002) Polygalacturonase-inhibiting proteins in defense against phytopathogenic fungi. *Curr. Opin. Plant Biol.* **5**, 295–299 https://doi.org/10.1016/S1369-5266(02)00271-6
37 Di Matteo, A., Federici, L., Mattei, B., Salvi, G., Johnson, K.A., Savino, C., et al. (2003) The crystal structure of polygalacturonase-inhibiting protein (PGIP), a leucine-rich repeat protein involved in plant defense. *Proc. Natl. Acad. Sci. U.S.A.* **100**, 10124–10128 https://doi.org/10.1073/pnas.1733690100
38 Zhang, D.Q., Liu, B., Feng, D.R., He, Y.M., Wang, S.Q., Wang, H.B., et al. (2004) Significance of conservative asparagine residues in the thermal hysteresis activity of carrot antifreeze protein. *Biochem. J.* **377**, 589–595 https://doi.org/10.1042/bj20031249
39 Otwinowski, Z. and Minor, W. (1997) Processing of X-ray diffraction data collected in oscillation mode. *Methods Enzymol.* **276**, 307–326 https://doi.org/10.1016/S0076-6879(97)76066-X

Biochemical Journal (2020) **477** 2179–2192
https://doi.org/10.1042/BCJ20200238

40 Mccoy, A.J., Grosse-Kunstleve, R.W., Adams, P.D., Winn, M.D., Storoni, L.C. and Read, R.J. (2007) Phaser crystallographic software. *J. Appl. Crystallogr.* **40**, 658–674 https://doi.org/10.1107/S0021889807021206
41 Emsley, P. and Cowtan, K. (2004) Coot: model-building tools for molecular graphics. *Acta Crystallogr. D Biol. Crystallogr.* **60**, 2126–2132 https://doi.org/10.1107/S0907444904019158
42 Emsley, P., Lohkamp, B., Scott, W.G. and Cowtan, K. (2010) Features and development of Coot. *Acta Crystallogr. D Biol. Crystallogr.* **66**, 486–501 https://doi.org/10.1107/S0907444910007493
43 Adams, P.D., Afonine, P.V., Bunkoczi, G., Chen, V.B., Davis, I.W., Echols, N., et al. (2010) PHENIX: a comprehensive Python-based system for macromolecular structure solution. *Acta Crystallogr. D Biol. Crystallogr* **66**, 213–221 https://doi.org/10.1107/S0907444909052925
44 Murshudov, G.N., Skubak, P., Lebedev, A.A., Pannu, N.S., Steiner, R.A., Nicholls, R.A., et al. (2011) REFMAC5 for the refinement of macromolecular crystal structures. *Acta Crystallogr. D Biol. Crystallogr.* **67**, 355–367 https://doi.org/10.1107/S0907444911001314
45 Stevens, C.A., Drori, R., Zalis, S., Braslavsky, I. and Davies, P.L. (2015) Dendrimer-linked antifreeze proteins have superior activity and thermal recovery. *Bioconjugate Chem.* **26**, 1908–1915 https://doi.org/10.1021/acs.bioconjchem.5b00290
46 Braslavsky, I. and Drori, R. (2013) LabVIEW-operated novel nanoliter osmometer for ice binding protein investigations. *J. Vis. Exp.* **72**, e4189 https://doi.org/10.3791/4189
47 Graham, L.A., Agrawal, P., Oleschuk, R.D. and Davies, P.L. (2018) High-capacity ice-recrystallization endpoint assay employing superhydrophobic coatings that is equivalent to the 'splat' assay. *Cryobiology* **81**, 138–144 https://doi.org/10.1016/j.cryobiol.2018.01.011
48 Vance, T.D.R., Graham, L.A. and Davies, P.L. (2018) An ice-binding and tandem beta-sandwich domain-containing protein in *Shewanella frigidimarina* is a potential new type of ice adhesin. *FEBS J.* **285**, 1511–1527 https://doi.org/10.1111/febs.14424
49 Zhang, D.Q., Wang, H.B., Liu, B., Feng, D.R., He, Y.M. and Wang, J.F. (2006) Carrot antifreeze protein does not exhibit the polygalacturonase-inhibiting activity of PGIP family. *Yi Chuan Xue Bao* **33**, 1027–1036 https://doi.org/10.1016/S0379-4172(06)60139
50 Garnham, C.P., Campbell, R.L. and Davies, P.L. (2011) Anchored clathrate waters bind antifreeze proteins to ice. *Proc. Natl. Acad. Sci. U.S.A.* **108**, 7363—7367 https://doi.org/10.1073/pnas.1100429108
51 Gronwald, W., Loewen, M.C., Lix, B., Daugulis, A.J., Sonnichsen, F.D., Davies, P.L., et al. (1998) The solution structure of type II antifreeze protein reveals a new member of the lectin family. *Biochemistry* **37**, 4712–4721 https://doi.org/10.1021/bi972788c
52 Jia, Z., DeLuca, C.I., Chao, H. and Davies, P.L. (1996) Structural basis for the binding of a globular antifreeze protein to ice. *Nature* **384**, 285–288 https://doi.org/10.1038/384285a0
53 Needleman, S.B. and Wunsch, C.D. (1970) A general method applicable to the search for similarities in the amino acid sequence of two proteins. *J. Mol. Biol.* **48**, 443–453 https://doi.org/10.1016/0022-2836(70)90057-4
54 Lauersen, K.J., Brown, A., Middleton, A., Davies, P.L. and Walker, V.K. (2011) Expression and characterization of an antifreeze protein from the perennial rye grass, *Lolium perenne*. *Cryobiology* **62**, 194–201 https://doi.org/10.1016/j.cryobiol.2011.03.003
55 Garnham, C.P., Gilbert, J.A., Hartman, C.P., Campbell, R.L., Laybourn-Parry, J. and Davies, P.L. (2008) A Ca^{2+}-dependent bacterial antifreeze protein domain has a novel beta-helical ice-binding fold. *Biochem. J.* **411**, 171–180 https://doi.org/10.1042/BJ20071372
56 Lin, F.H., Davies, P.L. and Graham, L.A. (2011) The Thr- and Ala-rich hyperactive antifreeze protein from inchworm folds as a flat silk-like beta-helix. *Biochemistry* **50**, 4467–4478 https://doi.org/10.1021/bi2003108